





# Study of rotor position estimation algorithm based on back-EMF voltage for dual-winding fault-tolerant permanent magnet motor

Yonghan Liu <sup>a</sup>, Jingwei Zhu <sup>a</sup>, Zhibin Wang <sup>a</sup> and Yan Liang <sup>b</sup>

<sup>a</sup>College of Marine Electrical Engineering, Dalian Maritime University, Dalian, People's Republic of China; <sup>b</sup>Hangzhou Subsidiary Company of Zhejiang Mobile Communication Limited Liability Company, Hangzhou, People's Republic of China

## ABSTRACT

An improved position estimation of the sensorless control system with online parameter identification based on back-Electromotive Force (EMF) voltage is presented for the dual-winding fault-tolerant permanent magnet motor (FTPMM). In this control system, the rotor position is estimated by the flux linkage and the back-EMF which are generated by each phase winding. By introducing phase-locked loop technology to compensate the steady-state error of the system and online identification of motor parameters which is using the least-square method with forgetting factor, more accurate position estimation can be obtained. The current vector fault-tolerant control strategy improves the fault tolerance of the system and makes it strong robust stability. The simulation results have shown that the accurate position data can be acquired both under healthy condition and single-phase fault condition. Then, the hardware experimental results show the feasibility and validity of the proposed algorithm.

## ARTICLE HISTORY

Received 12 February 2021  
Accepted 7 March 2022

## KEYWORDS

Dual-winding; fault-tolerant permanent magnet motor; sensorless control; back-EMF voltage; parameter identification

## Nomenclature

$u_A, u_B, u_C$	stator voltages in $A-B-C$ -axis
$u_{A0}, u_{B0}, u_{C0}$	stator voltages in $A0-B0-C0$ -axis
$i_A, i_B, i_C$	stator currents in $A-B-C$ -axis
$i_{A0}, i_{B0}, i_{C0}$	stator currents in $A0-B0-C0$ -axis
$e_A, e_B, e_C$	back electromotive force in $A-B-C$ -axis
$e_{A0}, e_{B0}, e_{C0}$	back electromotive force in $A0-B0-C0$ -axis
$L$	inductance
$k_e$	back electromotive force constant
$n_p$	Pole-pairs number
$\theta_e$	actual rotor electrical angle
$\Delta\theta_A, \Delta\theta_B, \Delta\theta_C,$ $\Delta\theta_{B0}, \Delta\theta_{C0}$	rotor position increments
$T$	sampling time
$\Delta\psi_A, \Delta\psi_B,$ $\Delta\psi_C, \Delta\psi_{A0},$ $\Delta\psi_{B0}, \Delta\psi_{C0}$	flux linkage increments
$\Delta i_A, \Delta i_B, \Delta i_C,$ $\Delta i_{A0}, \Delta i_{B0}, \Delta i_{C0}$	phase current increments
$\theta^*(k)$	predicted rotor position at sampling time $k$
$\theta(k-1)$	estimated rotor position at sampling time $(k-1)$
$\delta\theta_{AB}, \delta\theta_{BC},$ $\delta\theta_{CA}, \delta\theta_{A0B0},$ $\delta\theta_{B0C0}, \delta\theta_{C0A0}$	phase difference between the phase angle of flux linkage increment and the estimated rotor position
$K_f$	phase detector gain $\sqrt{3} \Delta\psi /2$

$K_p$	proportional gain
$K_i$	integral gain
$\omega_e$	angular velocity of the motor
$\psi_f$	permanent magnet flux linkage
$u_d, u_q$	$d$ -axis and $q$ -axis stator voltages
$i_d, i_q$	$d$ -axis and $q$ -axis stator currents
$T_0$	output torque

## 1. Introduction

Recently, the fault-tolerant permanent magnet machine has been proposed, which offers high-power density, excellent electrical and magnetic isolation capability and good fault tolerance capability. The dual-winding fault-tolerant permanent magnet motor (FTPMM) has two sets of independent three-phase concentrated armature windings on alternate teeth [1]. Combined with the excellent characteristics of FTPMM and double-redundancy control system, it has the advantages of large space utilization rate, high reliability and low cost, which has attracted wide attention of scholars. In traditional motor position detection system, the rotor position can be obtained by photoelectric encoder, rotary transformer and other devices, which inevitably increase the complexity and affect the dynamic and static performance of the system [2]. It goes against the original intention of designing dual-winding FTPMM to enhance the system reliability. Therefore, the study of estimating

the rotor position of dual-winding FTPMM that can improve its accuracy and stability has important implications.

In recent years, a variety of rotor position estimation algorithms have been proposed, such as model reference adaptive method [3,4], observer method [5–7], high-frequency signal injection method [8–10], artificial intelligence method [11,12], and back-EMF method [13,14]. In the literature [3], the model reference adaptive system was proposed to obtain better rotor position information at low speed, but it is sensitive to the change of motor parameters. The robustness of the observer estimation in the paper [5] performed better, but its calculation is large and the algorithm is complex. The high-frequency signal injection method used in the literature can achieve the estimation of the initial position of the rotor at zero speed [8]. But the saliency effect inside the motor which is one of the necessary conditions for using this method is difficult to realize on the motor with a surface-mounted rotor structure. The artificial intelligence method is relatively cutting-edge and has strong adaptive ability. However, the algorithm is complex and it is far from being practical. The back-EMF method is relatively simple and flexible. Compared with other traditional control methods, drive with back-EMF-based sensorless control that is proposed in Ref. [15] gives the better dynamic response.

The position estimation is not accurate due to the influence of temperature and sampling frequency. Besides, the phase delay caused by the use of LPF will also bring errors to the position estimation. Therefore, phase-locked loop (PLL) is being widely used in conjunction with position estimation methods for its relatively simple frame to overcome the drawbacks that are mentioned before [16–18]. Back-EMF-based phase locked loop (PLL) method has been extensively researched for PMSM sensorless control and more accurate technique for rotor position estimation has been created. A novel finite-position-set PLL is used for a surface-mounted PMSM in Ref. [16], which provides a limited position angle for calculating back-EMF. The method itself has good robust performance. The estimated back EMFs of no fault two phases are usually nonorthogonal in FTPMM. In Ref. [18], the nonorthogonal PLL is proposed to calculate the rotor position using back-EMF of any two phases. This control guaranteed the rotor position estimation performance of the FTPMSM in normal and in fault conditions.

Compared with PMSM, the dual-winding FTPMM consists of isolated inter-windings which are driven by a three-phase H-bridge inverter circuit, so the sensorless position estimation algorithm mentioned above cannot be used directly. Based on the method proposed in

Ref. [19], an improved scheme for position estimation of back-EMF is presented, which is applicable for dual-winding FTPMM. Since the accuracy is greatly affected by the variation of motor parameters (inductance and resistance), the recursive least-square with forgetting factor method proposed in the literature [20] is applied to the online identification of inductance and resistance of the motor. In this algorithm, all the identification results are updated in real time. The veracity of the rotor position estimation method of the dual-winding FTPMM is testified by MATLAB/Simulink under the condition of normal motor operation, one-phase fault and two-phase fault. Finally, an experimental platform is built to testify the accuracy and efficiency of the proposed algorithm.

## 2. Mathematical model of dual-winding FTPMM

The proposed dual-winding FTPMM consists of a surface-mounted permanent magnet rotor and two sets of windings. It adopts the structure of stator core with teeth groove and single-layer concentrated winding. The thermal isolation, physical isolation and magnetic isolation can be realized by the isolated teeth between each winding, which can inhibit the influence of short circuit current and improve the fault-tolerant performance [21]. Figure 1 shows the structure of the dual-winding three-phase, 12 slots and 8 poles FTPMM. The back-EMF waveform of phase A, B and C of the difference is between  $120^\circ$ , the same as phase A0, B0 and C0.

As is shown in Figure 2, every phase drives by an independent H-bridge. The independent H-bridge can eliminate the electrical coupling between phase windings and increases the utilization of DC power supply, making it possible to measure the position in case of the motor breaking down.

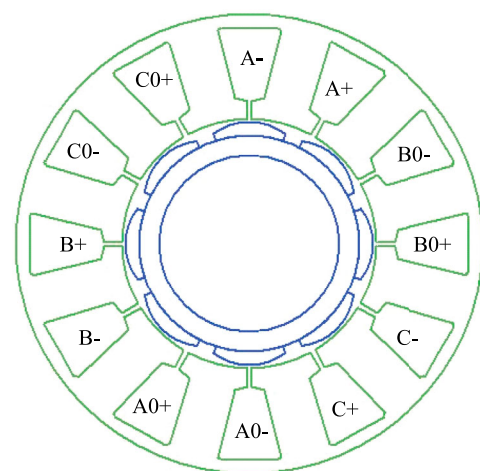
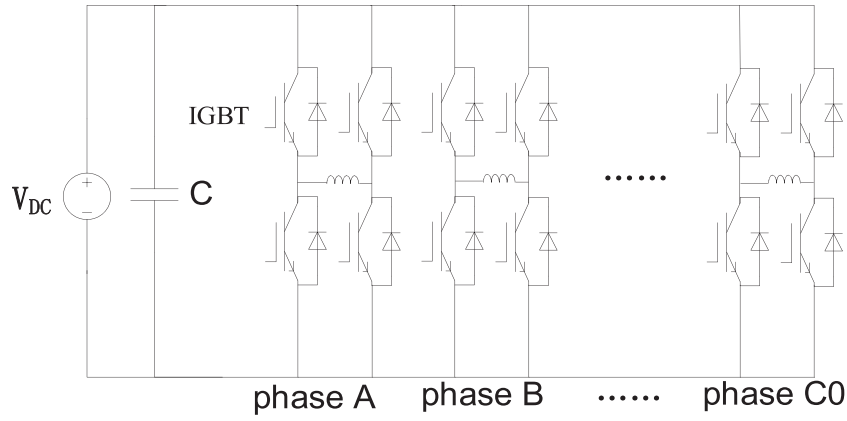


Figure 1. The structure of dual-winding FTPMM.



**Figure 2.** The main circuit of dual-winding FTPMM.

The voltage equation of each phase winding is given by the following equation:

$$\begin{bmatrix} u_A \\ u_B \\ u_C \\ u_{A0} \\ u_{B0} \\ u_{C0} \end{bmatrix} = \begin{bmatrix} R & 0 & 0 & 0 & 0 & 0 \\ 0 & R & 0 & 0 & 0 & 0 \\ 0 & 0 & R & 0 & 0 & 0 \\ 0 & 0 & 0 & R & 0 & 0 \\ 0 & 0 & 0 & 0 & R & 0 \\ 0 & 0 & 0 & 0 & 0 & R \end{bmatrix} \begin{bmatrix} i_A \\ i_B \\ i_C \\ i_{A0} \\ i_{B0} \\ i_{C0} \end{bmatrix} + \begin{bmatrix} L & 0 & 0 & 0 & 0 & 0 \\ 0 & L & 0 & 0 & 0 & 0 \\ 0 & 0 & L & 0 & 0 & 0 \\ 0 & 0 & 0 & L & 0 & 0 \\ 0 & 0 & 0 & 0 & L & 0 \\ 0 & 0 & 0 & 0 & 0 & L \end{bmatrix} \frac{d}{dt} \begin{bmatrix} i_A \\ i_B \\ i_C \\ i_{A0} \\ i_{B0} \\ i_{C0} \end{bmatrix} + \frac{k_e}{n_p} \frac{d\theta_e}{dt} \begin{bmatrix} e_A \\ e_B \\ e_C \\ e_{A0} \\ e_{B0} \\ e_{C0} \end{bmatrix}. \quad (1)$$

### 3. Rotor position estimation algorithm

Since the two sets of stator windings correspond to the same axis, the six rotor position increments  $\Delta\theta_i$  ( $i = A, B, C, A0, B0, C0$ ) should be equal. When the sampling frequency is high enough (the frequency is set as 10 kHz in the simulation and experiment), formula (1) can be derived to represent the increment of rotor position as follows (take phase A, for example). The same as other rotor position increment.

$$\frac{d\theta_e}{dt} = \frac{n_p}{k_e e_A} \left( u_A - R i_A - L \frac{d i_A}{dt} \right), \quad (2)$$

$$\Delta\theta_A = \frac{n_p}{k_e} \frac{(u_A - R i_A) T - L \Delta i_A}{e_A} = \frac{n_p}{k_e} \frac{\Delta\psi_A}{e_A}. \quad (3)$$

The zero-crossing of each back-EMF will increase the estimation error of position increment since the back-EMF is sinusoidal. In order to avoid such a situation, this paper makes an improvement on the basis of

the literature [13] and proposes a fault-tolerant control method of dual-winding FTPMM. When a two-phase fault occurs in the motor, such as open or short circuit fault in phase A and A0,  $\Delta\theta_A$  and  $\Delta\theta_{A0}$  cannot be detected due to the loss of current  $i_A$  and  $i_{A0}$ . This paper uses a selective scheme to acquire the increments of rotor position [22]. It is done by multiplying both sides of the formula (3) by  $e_A^2$ ,  $e_B^2$ ,  $e_C^2$ ,  $e_{A0}^2$ ,  $e_{B0}^2$  and  $e_{C0}^2$ , respectively. The resulting Equation (4) which represents the estimated position increments is the sum of two adjacent phases.

$$\begin{bmatrix} \Delta\theta_{AB} \\ \Delta\theta_{BC} \\ \Delta\theta_{CA} \\ \Delta\theta_{A0B0} \\ \Delta\theta_{B0C0} \\ \Delta\theta_{C0A0} \end{bmatrix} = \frac{n_p}{k_e} \begin{bmatrix} \frac{\Delta\psi_A e_A + \Delta\psi_B e_B}{e_A^2 + e_B^2} \\ \frac{\Delta\psi_B e_B + \Delta\psi_C e_C}{e_B^2 + e_C^2} \\ \frac{\Delta\psi_C e_C + \Delta\psi_A e_A}{e_C^2 + e_A^2} \\ \frac{\Delta\psi_{A0} e_{A0} + \Delta\psi_{B0} e_{B0}}{e_{A0}^2 + e_{B0}^2} \\ \frac{\Delta\psi_{B0} e_{B0} + \Delta\psi_{C0} e_{C0}}{e_{B0}^2 + e_{C0}^2} \\ \frac{\Delta\psi_{C0} e_{C0} + \Delta\psi_{A0} e_{A0}}{e_{C0}^2 + e_{A0}^2} \end{bmatrix}. \quad (4)$$

From the squared terms of the denominator on the right side of formula (4), it can be seen that its value is always greater than 0. It can avoid the infinitely increasing zero-crossing errors of the back-EMF function.

$$\begin{cases} \theta_{AB}^*(k) = \theta_{AB}(k-1) + \Delta\theta_{AB}, \\ \theta_{BC}^*(k) = \theta_{BC}(k-1) + \Delta\theta_{BC}, \\ \theta_{CA}^*(k) = \theta_{CA}(k-1) + \Delta\theta_{CA}, \\ \theta_{A0B0}^*(k) = \theta_{A0B0}(k-1) + \Delta\theta_{A0B0}, \\ \theta_{B0C0}^*(k) = \theta_{B0C0}(k-1) + \Delta\theta_{B0C0}, \\ \theta_{C0A0}^*(k) = \theta_{C0A0}(k-1) + \Delta\theta_{C0A0}. \end{cases} \quad (5)$$

Table 1 lists the rotor position information available when the dual-winding FTPMM is operating in healthy and different faulty conditions. As shown in the table, if the drive works properly, the position estimation can be acquired directly by using the average value

**Table 1.** Dual-winding FTPMM operating conditions and standby rotor information sheet.

The working state of dual-winding FTPMM	Available rotor position information	The final estimated rotor position $\theta(k)$
Healthy condition	$\theta_{BC}, \theta_{CA}, \theta_{AB}, \theta_{A0B0}, \theta_{B0C0}, \theta_{C0A0}$	$(\theta_{BC} + \theta_{CA} + \theta_{AB} + \theta_{A0B0} + \theta_{B0C0} + \theta_{C0A0})/6$
Phase A fault	$\theta_{BC}, \theta_{A0B0}, \theta_{B0C0}, \theta_{C0A0}$	$(\theta_{BC} + \theta_{A0B0} + \theta_{B0C0} + \theta_{C0A0})/4$
Phase B fault	$\theta_{CA}, \theta_{A0B0}, \theta_{B0C0}, \theta_{C0A0}$	$(\theta_{CA} + \theta_{A0B0} + \theta_{B0C0} + \theta_{C0A0})/4$
Phase C fault	$\theta_{AB}, \theta_{A0B0}, \theta_{B0C0}, \theta_{C0A0}$	$(\theta_{AB} + \theta_{A0B0} + \theta_{B0C0} + \theta_{C0A0})/4$
Phase A and B fault	$\theta_{A0B0}, \theta_{B0C0}, \theta_{C0A0}$	$(\theta_{A0B0} + \theta_{B0C0} + \theta_{C0A0})/3$
Phase B and C fault	$\theta_{A0B0}, \theta_{B0C0}, \theta_{C0A0}$	$(\theta_{A0B0} + \theta_{B0C0} + \theta_{C0A0})/3$
Phase C and A fault	$\theta_{A0B0}, \theta_{B0C0}, \theta_{C0A0}$	$(\theta_{A0B0} + \theta_{B0C0} + \theta_{C0A0})/3$
Phase A and A0 fault	$\theta_{BC}, \theta_{B0C0}$	$(\theta_{BC} + \theta_{B0C0})/2$
Phase A and B0 fault	$\theta_{BC}, \theta_{C0A0}$	$(\theta_{BC} + \theta_{C0A0})/2$
Phase A and C0 fault	$\theta_{BC}, \theta_{A0B0}$	$(\theta_{BC} + \theta_{A0B0})/2$

of six available rotor position estimates. Only four rotor positions can be estimated under the circumstance that one-phase fault. If a two-phase failure occurs within the same motor module, then the rotor position estimation can be acquired from the three estimates of another intact motor module. Finally, if a single-phase failure in both modules, then only two position estimates are available.

Ideally, the rotor position estimates can be acquired by averaging the available rotor positions. However, in practice, there is a steady-state error which is influenced by the inaccurate data or/and time delays between the estimated rotor position and the actual rotor position, namely, the phase difference which is influenced by the inaccurately measured voltage and current data. Besides, the variation of motor parameters is susceptible to temperature changes, limited sampling frequency and other factors will also affect the estimation results. In consequence, an improved PLL technology was adopted that allows the predicted rotor position to track the flux linkage increments of the corresponding phases which can compensate for this steady-state error [23].

For a motor, the back-EMF is proportional to the rate of flux linkage change, that is, the back-EMF is also proportional to the flux increment. Therefore, for each phase, the back-EMF which corresponds to the estimated rotor position and the measured flux linkage increment should be in the same phase.

Formula (6) is a vector product represented by flux linkage increment and back-EMF. It shows the mathematical expressions in the PLL technique above.

$$\begin{aligned}
 & \begin{bmatrix} \|\Delta\vec{\psi}_1 \times \vec{e}_1\|_{AB} \\ \|\Delta\vec{\psi}_2 \times \vec{e}_2\|_{BC} \\ \|\Delta\vec{\psi}_3 \times \vec{e}_3\|_{CA} \\ \|\Delta\vec{\psi}_4 \times \vec{e}_4\|_{A0B0} \\ \|\Delta\vec{\psi}_5 \times \vec{e}_5\|_{B0C0} \\ \|\Delta\vec{\psi}_6 \times \vec{e}_6\|_{C0A0} \end{bmatrix} \\
 &= \begin{bmatrix} \Delta\psi_A e_B(\theta_{AB}^*) - \Delta\psi_B e_A(\theta_{AB}^*) \\ \Delta\psi_B e_C(\theta_{BC}^*) - \Delta\psi_C e_B(\theta_{BC}^*) \\ \Delta\psi_C e_A(\theta_{CA}^*) - \Delta\psi_A e_C(\theta_{CA}^*) \\ \Delta\psi_{A0} e_{B0}(\theta_{A0B0}^*) - \Delta\psi_{B0} e_{A0}(\theta_{A0B0}^*) \\ \Delta\psi_{B0} e_{C0}(\theta_{B0C0}^*) - \Delta\psi_{C0} e_{B0}(\theta_{B0C0}^*) \\ \Delta\psi_{C0} e_{A0}(\theta_{C0A0}^*) - \Delta\psi_{A0} e_{C0}(\theta_{C0A0}^*) \end{bmatrix}
 \end{aligned}$$

$$\begin{aligned}
 &= \frac{\sqrt{3}}{2} * |\Delta\psi| \begin{bmatrix} \sin(\theta_{\psi f} - \theta_{AB}^*) \\ \sin(\theta_{\psi f} - \theta_{BC}^*) \\ \sin(\theta_{\psi f} - \theta_{CA}^*) \\ \sin(\theta_{\psi f} - \theta_{A0B0}^*) \\ \sin(\theta_{\psi f} - \theta_{B0C0}^*) \\ \sin(\theta_{\psi f} - \theta_{C0A0}^*) \end{bmatrix} \\
 &\approx K_f \begin{bmatrix} \theta_{\psi f} - \theta_{AB}^* \\ \theta_{\psi f} - \theta_{BC}^* \\ \theta_{\psi f} - \theta_{CA}^* \\ \theta_{\psi f} - \theta_{A0B0}^* \\ \theta_{\psi f} - \theta_{B0C0}^* \\ \theta_{\psi f} - \theta_{C0A0}^* \end{bmatrix} = K_f \begin{bmatrix} \delta\theta_{AB}(k) \\ \delta\theta_{BC}(k) \\ \delta\theta_{CA}(k) \\ \delta\theta_{A0B0}(k) \\ \delta\theta_{B0C0}(k) \\ \delta\theta_{C0A0}(k) \end{bmatrix}. \quad (6)
 \end{aligned}$$

Therefore, the estimated rotor position between two phases after steady-state error compensation can be expressed as

$$\begin{aligned}
 & \begin{bmatrix} \theta_{AB}(k) \\ \theta_{BC}(k) \\ \theta_{CA}(k) \\ \theta_{A0B0}(k) \\ \theta_{B0C0}(k) \\ \theta_{C0A0}(k) \end{bmatrix} \\
 &= \begin{bmatrix} \theta_{AB}^*(k) + K_f(K_p \delta\theta_{AB}(k) \\ + K_i \sum_{i=0}^k \delta\theta_{AB}(i)) \\ \theta_{BC}^*(k) + K_f(K_p \delta\theta_{BC}(k) \\ + K_i \sum_{i=0}^k \delta\theta_{BC}(i)) \\ \theta_{CA}^*(k) + K_f(K_p \delta\theta_{CA}(k) \\ + K_i \sum_{i=0}^k \delta\theta_{CA}(i)) \\ \theta_{A0B0}^*(k) + K_f(K_p \delta\theta_{A0B0}(k) \\ + K_i \sum_{i=0}^k \delta\theta_{A0B0}(i)) \\ \theta_{B0C0}^*(k) + K_f(K_p \delta\theta_{B0C0}(k) \\ + K_i \sum_{i=0}^k \delta\theta_{B0C0}(i)) \\ \theta_{C0A0}^*(k) + K_f(K_p \delta\theta_{C0A0}(k) \\ + K_i \sum_{i=0}^k \delta\theta_{C0A0}(i)) \end{bmatrix}. \quad (7)
 \end{aligned}$$

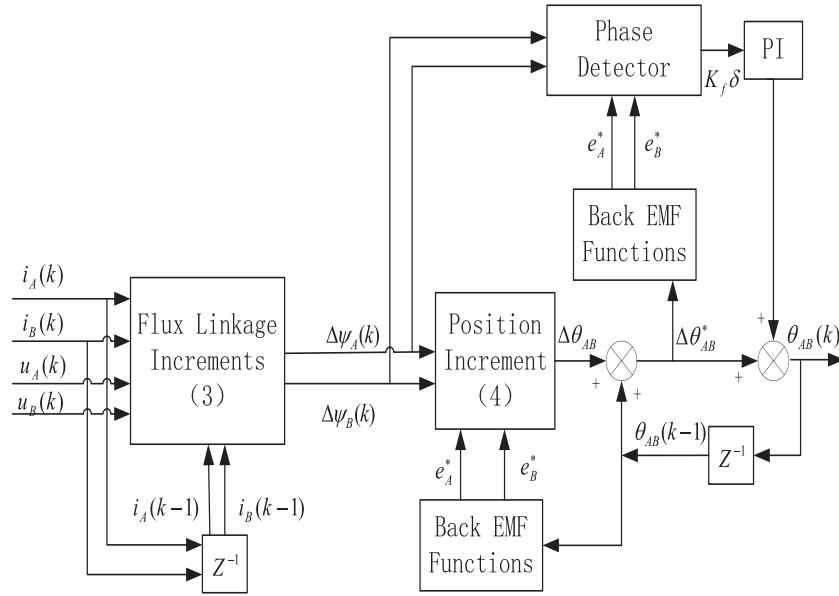


**Figure 3.** The diagram of the estimated rotor position for a pair of phases *A* and *B* of the dual-winding FTPMM.

The diagram of position increment estimation algorithm for *A* and *B* of the motor module is shown in Figure 3. The back-EMF and flux linkage increment of the adjacent phase *A* and *B* is taken as an input, passing the phase difference which is obtained through a Proportion Integral (PI) regulator to form a modified PLL, then added to the predicted value of rotor position to compensate for the steady-state error.

#### 4. Online identification of motor parameters

The accuracy of the estimation algorithm is affected by motor parameters  $R$ ,  $L$  and  $\psi_f$ . During the motor operation, the electrical parameters will change with various environmental factors, such as the stator resistance and flux linkage will be influenced by temperature and the inductance will vary with magnetic saturation [24]. If the rotor position estimation algorithm cannot recognize this change, the accuracy of position estimation results will be affected directly. Therefore, parameters  $R$ ,  $L$  and  $\psi_f$  should be identified online in a correct way.

##### 4.1. The least-square parameter identification

The equation of state of the system can be expressed as

$$Y(k) = \Theta * X(k), \quad (8)$$

where  $Y$  is the system output variable,  $\Theta$  is the parameter to be identified and  $X$  is the system input variable.

Since there will be a deviation  $E(k)$  between the actual value and the estimated value in the identification process, the output can be corrected as

$$Y(k) = \hat{\Theta} * X(k) + E(k). \quad (9)$$

The error vector is assumed as

$$E(k) = [e(1) \quad e(2) \quad \dots \quad e(k)]^T. \quad (10)$$

According to the least-square method, the identification result is optimal when the sum of squares of errors is minimum [25].

$$F = \sum_{i=1}^k e_i^2 = E_k^T E_k. \quad (11)$$

The relationship between  $\Theta$  and  $F$  can be derived from the expansion (12)

$$\begin{aligned} F &= (Y - X\hat{\Theta})^T (Y - X\hat{\Theta}) \\ &= Y^T Y - \hat{\Theta}^T X^T Y - Y^T X \hat{\Theta} + \hat{\Theta}^T X^T X \hat{\Theta}. \end{aligned} \quad (12)$$

Differentiating  $F$  with respect to  $\hat{\Theta}$  to make sure that  $F$  is the minimum value, set the derivative to zero.

$$\frac{\partial F}{\partial \hat{\Theta}} = -2X^T Y + 2X^T X \hat{\Theta} = 0, \quad (13)$$

$$\hat{\Theta} = (X^T X)^{-1} X^T Y. \quad (14)$$

##### 4.2. The forgetting factor recursive least-square parameter identification

The least-square parameter identification method can be used to obtain the identification results under the condition of motor parameters change. But in practice, the data at the previous moment should be substituted into the calculation again when a new observation is made. This will increase the computational load and decrease the computational efficiency obviously. Therefore, the forgetting factor recursive least-square method is introduced in this paper, which can use the previous identification results directly in the new observation, reduce the computational load and improve the efficiency.

The recursive matrix  $P$  is introduced for real-time estimation:

$$P(k+1) = \frac{1}{\lambda} \left[ P(k) - \frac{P(k)X(k+1)X(k+1)^T P(k)}{\lambda + X^T(k+1)P(k)X(k+1)} \right]. \quad (15)$$

Here,  $\lambda$  is the forgetting factor that represents the impact of historical data on the current moment,  $\lambda < 1$ .

The smaller the  $\lambda$ , the faster the recursive square method converges. But it will be difficult to converge if the  $\lambda$  is configured too small, so the convergence rate and stability of the estimated value should be considered for the selection of  $\lambda$  [26].

The parameter estimation recursion can be expressed as follows after the introduction of  $P$ :

$$\hat{\Theta}(k+1) = \hat{\Theta}(k) + \frac{P(k)X(k+1)}{\lambda + X^T(k+1)P(k)X(k+1)} \cdot [Y(k+1) - X^T(k+1)\hat{\Theta}(k)]. \quad (16)$$

The motor's parameters phase inductance, phase resistance and flux need to be identified online since the rotor position estimation algorithm in the last section is greatly affected. Equations (17) and (18) are the dynamic mathematical model of the dual-winding FTPMM in the d-q two-phase rotating coordinate system

$$\frac{di_d}{dt} - \omega_e i_q = -\frac{R}{L} i_d + \frac{1}{L} u_d, \quad (17)$$

$$\frac{di_q}{dt} + \omega_e i_d = -\frac{R}{L} i_q - \frac{\psi_f}{L} \omega_e + \frac{1}{L} u_q. \quad (18)$$

Parameter identification matrix for estimating  $R$ ,  $L$  and  $\psi_f$  can be formulated from Equations (17) and (18) as shown below:

$$\frac{di_d}{dt} + \omega_e i_d = [-i_q \quad -\omega_e \quad u_q] \begin{bmatrix} \frac{R}{L} \\ \frac{\psi_f}{L} \\ \frac{1}{L} \end{bmatrix}, \quad (19)$$

$$\frac{di_q}{dt} + \omega_e i_q = [-i_q \quad -\omega_e \quad u_q] \begin{bmatrix} a \\ b \\ c \end{bmatrix}, \quad (20)$$

where

$$a = \frac{R}{L}, b = \frac{\psi_f}{L} \text{ and } c = \frac{1}{L}, \quad (21)$$

$$R = \frac{a}{c}, L = \frac{1}{c} \text{ and } \psi_f = \frac{b}{c}. \quad (22)$$

From Equation (22), the motor's parameters  $R$ ,  $L$  and  $\psi_f$  can be estimated by knowing  $a$ ,  $b$  and  $c$ .

Let  $y(k) = (di_d/dt) + \omega_e i_d$ ,  $x_1 = i_q$ ,  $x_2 = -\omega_e$ ,  $x_3 = u_q$ . The following data can be obtained through  $k$  observations:

$$Y_k = \begin{bmatrix} y(1) \\ y(2) \\ \vdots \\ y(m) \end{bmatrix}, X_k = \begin{bmatrix} x_1(1) & x_2(1) & x_3(1) \\ x_1(2) & x_2(2) & x_3(2) \\ \vdots & \vdots & \vdots \\ x_1(k) & x_2(k) & x_3(k) \end{bmatrix}, \Theta = \begin{bmatrix} a \\ b \\ c \end{bmatrix}.$$

The online identification results of  $R$ ,  $L$  and  $\psi_f$  can be obtained by substituting into Equations (15) and (16). The robustness of the position estimation algorithm can be improved by updating the identification results to the rotor position estimation algorithm in the previous section.

## 5. Simulation verification

The FTPMM is an independent centralized winding stator structure, and every independent H-bridge inverter drives one phase of the motor. Therefore, the initial position information of the rotor can be obtained directly by using the back-EMF control algorithm regardless of the occurrence of faults. When fault condition occurs in the dual-winding FTPMM, two sets of stator windings are symmetrically connected. It can be seen from the relationship between motor current and torque in formula (23) that the output torque of the motor can be controlled by controlling the current of each phase winding directly. When short or open-circuit faults occur (take phase A as example), the output torque of the motor will be reduced. In order to compensate the output torque, an improved method of fault-tolerant control based on current vectors is used in this article [27].

$$T_O = \frac{1}{\omega_e} (e_A i_A + e_B i_B + e_C i_C + e_{A0} i_{A0} + e_{B0} i_{B0} + e_{C0} i_{C0}). \quad (23)$$

Its principle is the application of other fault-free current vectors to compensate the fault current vectors. The structure of the vector fault-tolerant control system is shown in Figure 4. The position sensorless control system mainly consists of fault judgement, reference current calculation, speed calculation and current/voltage detection.

Matlab/simulink is used to simulate the rotor position estimation algorithm of dual-winding FTPMM, including healthy and faulty conditions. The motor is controlled by PI regulator and current hysteresis band Pulse-Width Modulation (PWM) control. Table 2 shows the parameters of the motor used in the simulation. The sampling frequency is set to 10 kHz.

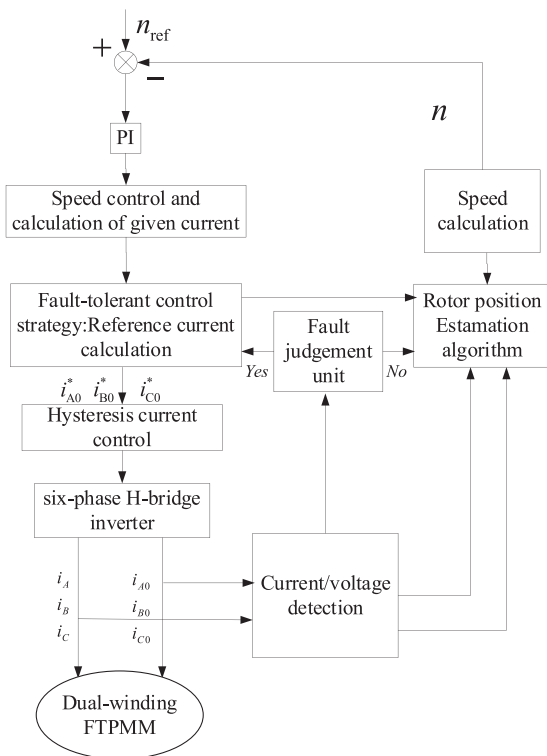


**Figure 4.** Structure diagram of the position sensorless control system with the tactic of current vector in FTPMM.

**Table 2.** The motor parameters.

Parameters	Value
Stator resistance, $R$ ( $\Omega$ )	1.2
Number of pole-pairs, $np$	4
Winding inductance, $L$ (mH)	27.42
Damping coefficient, $B$	0
Moment of inertia, $J$ ( $\text{kg m}^2$ )	0.0097
Back-EMF constant, $k_e$ ( $\text{V rad s}^{-1}$ )	0.417

**5.1. Simulation of rotor position estimation algorithm without parameter identification**

The dual-winding FTPMM runs at a constant load torque of 5 N m, 100 v DC voltage and 15 A reference current amplitude. The waveform of simulation results of the rotor position estimation algorithm without parameter  $R$  and  $L$  identification function is shown in Figure 5, which makes the motor parameter value fluctuate by 15% in 0.25 s. It can be seen from the figure that the estimated error before parameter change is within 0.1 rad, which is relatively accurate. But the error is shifted downward to 0.01 rad after 0.25 s. Therefore, the accuracy of the rotor position estimation method without parameter identification function will be influenced by the parameter changes in the actual working process of the motor.

**5.2. Simulation of rotor position estimation algorithm with parameter identification**

In order to eliminate the influence of motor parameters  $R$  and  $L$  on rotor position estimation, an online parameter identification method based on back-EMF is introduced in the estimation algorithm. Based on the parameter identification, corresponding improvements are made to improve the veracity of the position estimation algorithm in this paper. Therefore, the forgetting factor recursive least-square method is introduced. Online identification of the motor parameters  $R$  and  $L$  using the least-square method with forgetting factor is helpful to reduce the estimated error and can also improve the control precision of the dual-winding FTPMM.

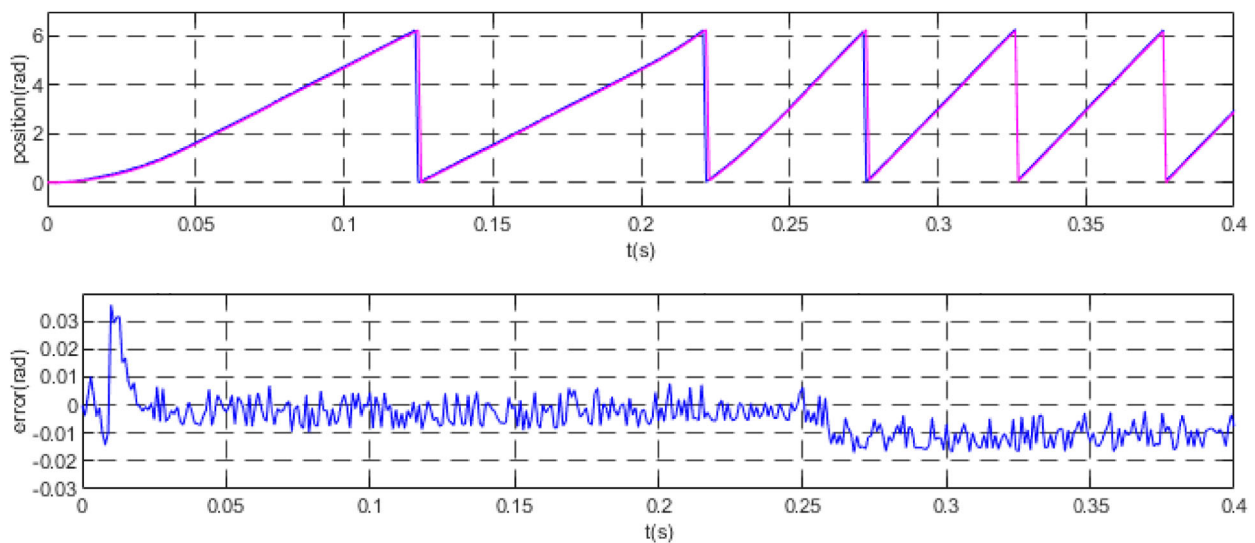


**Figure 5.** The simulation waveform of the speed step change under the condition of no parameter identification. (a) The estimated rotor position and the actual position: blue trace (estimated position), purple trace (actual position) and (b) the error of the estimated rotor position.

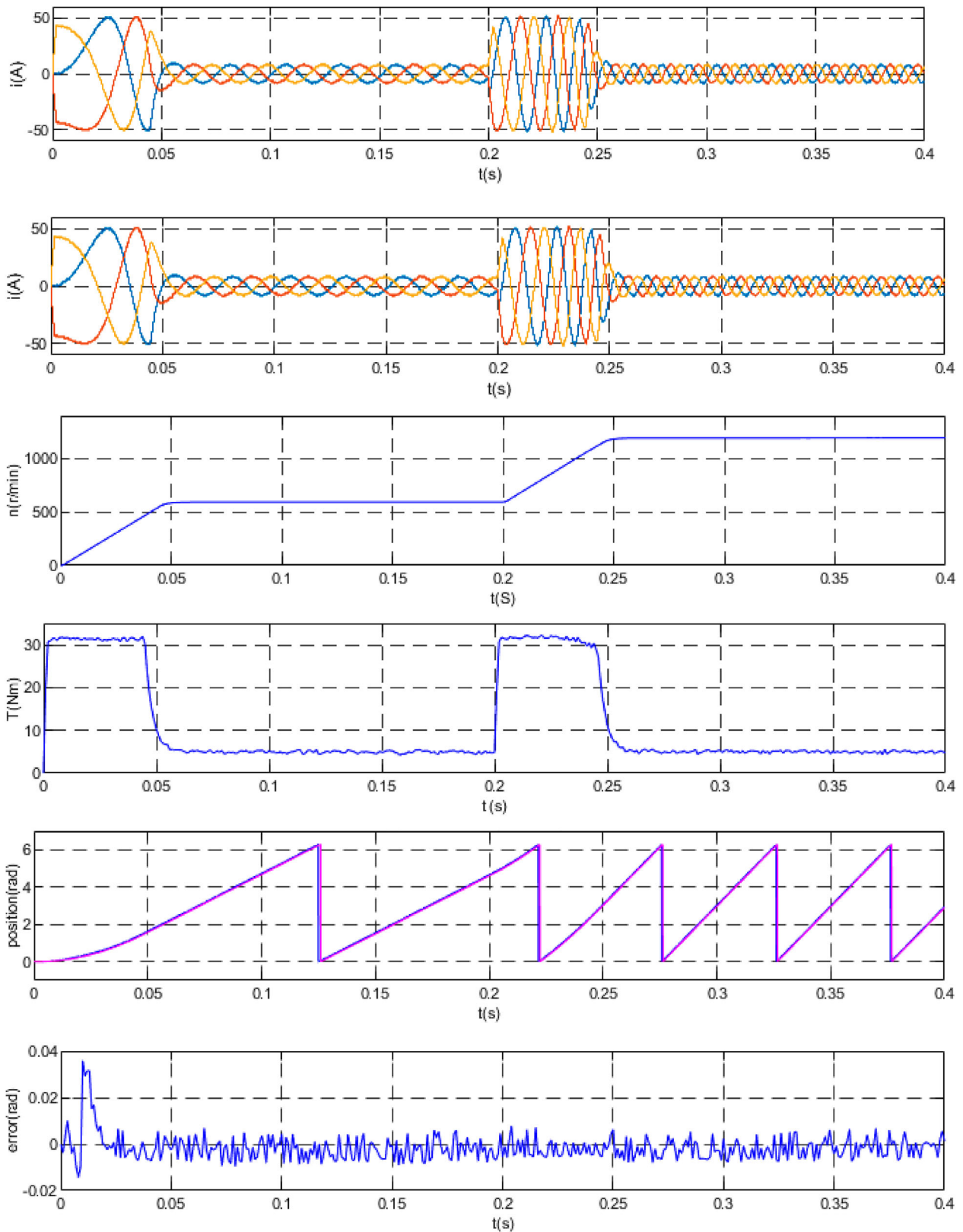


**Figure 6.** The simulation waveform of the speed step change under the condition of no fault. (a) The oscillograph of current of phase A, B, C: blue trace (A), red trace (B), yellow trace (C). (b) The oscillograph of current of phase A0, B0, C0: blue trace (A0), red trace (B0), yellow trace (C0). (c) The actual speed. (d) The electromagnetic torque. (e) The estimated rotor position and the actual position: blue trace (estimated position), purple trace (actual position). (f) The error of the estimated rotor position.

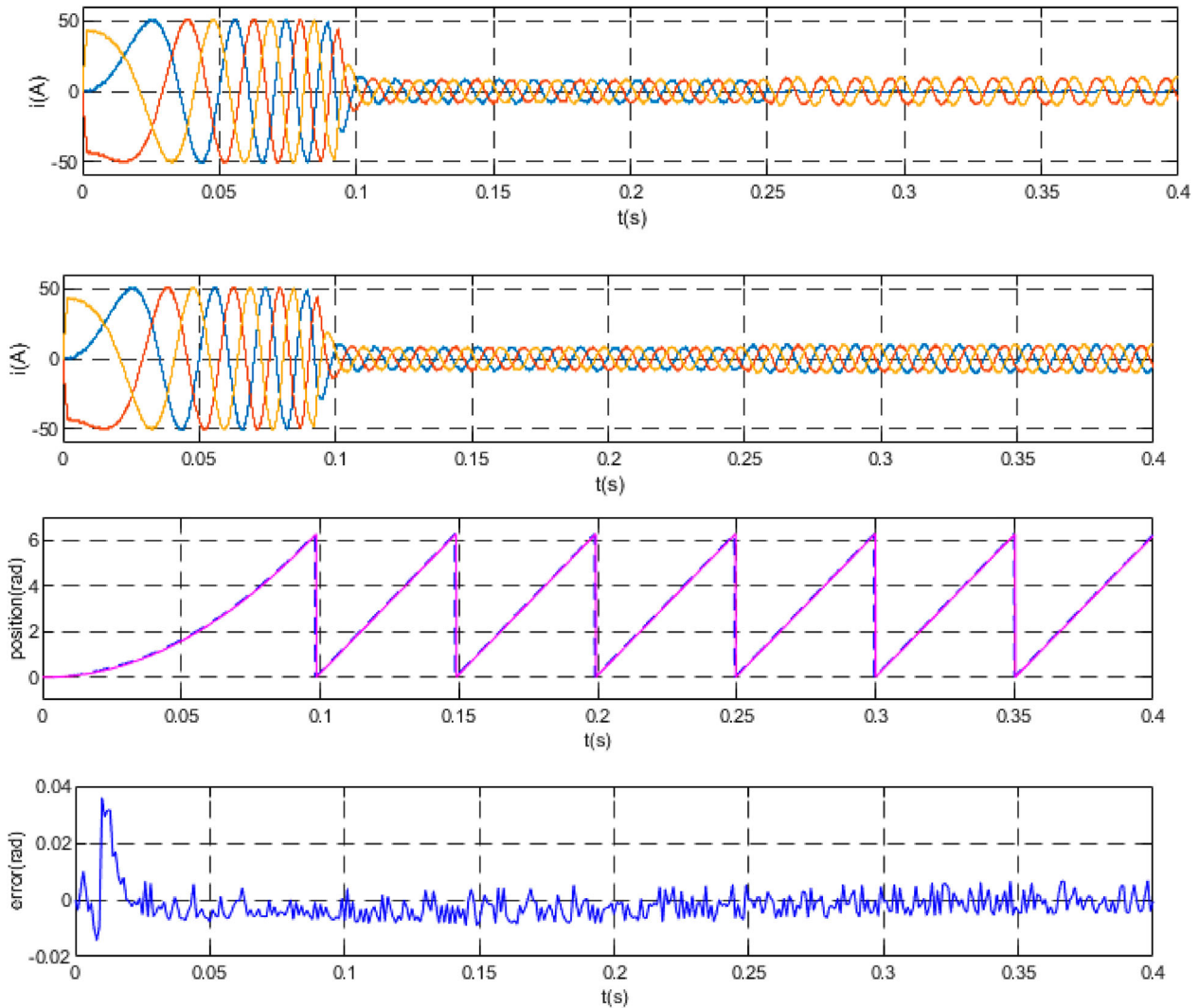


**Figure 7.** The simulation waveform of the speed step change under single-phase open-circuit fault condition. (a) The oscillograph of current of phase A, B, C: blue trace (A), red trace (B), yellow trace (C). (b) The oscillograph of current of phase A0, B0, C0: blue trace (A0), red trace (B0), yellow trace (C0). (c) The estimated rotor position and the actual position: blue trace (estimated position), purple trace (actual position). (d) The error of the estimated rotor position.

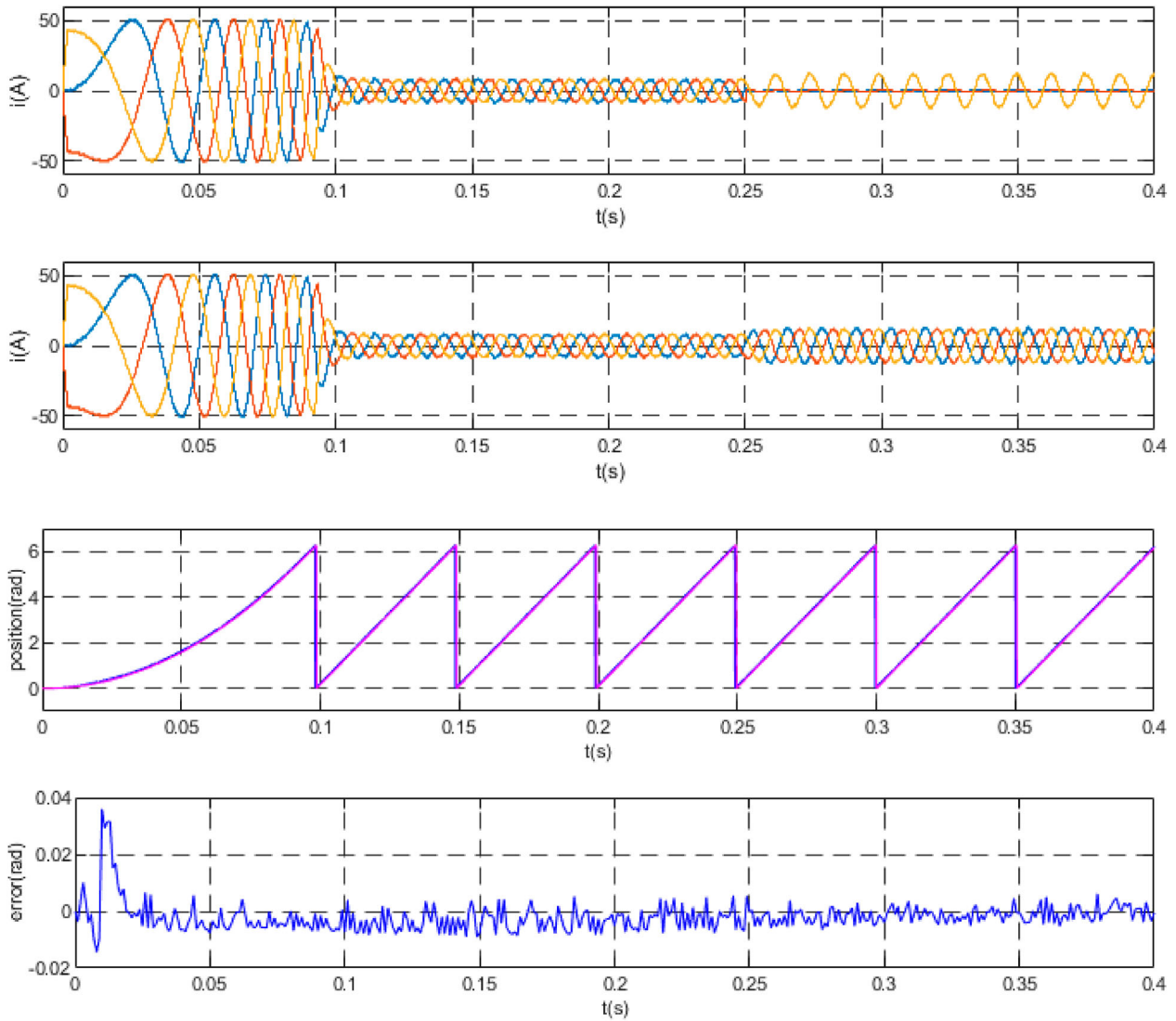
Figure 6 shows the online identification results of parameters updated to the position estimation algorithm in the case of no fault of the motor. The dual-winding FTPMM runs at a constant load torque of 5 N m. The simulation waveform was obtained by the given speed from 600 r/min steps to 1200 r/min at 0.2 s. There are some fluctuations in the current when the motor is started and tends to stabilize in about 0.04 s. At 0.2 s, the actual position is very close to the position estimation when the motor speed steps from 600 r/min to 1200 r/min. The rotor position estimation errors were  $\pm 0.05$  rad and  $\pm 0.1$  rad, respectively, when the motor speed is at 1200 r/min and 600 r/min, indicating that the estimated position could well follow the actual position.

Figure 7 shows the simulation results of the rotor position estimation algorithm when the online identification function of motor parameters is adopted under the condition of one-phase open-circuit fault of the motor. It can be seen from the figure that the remaining

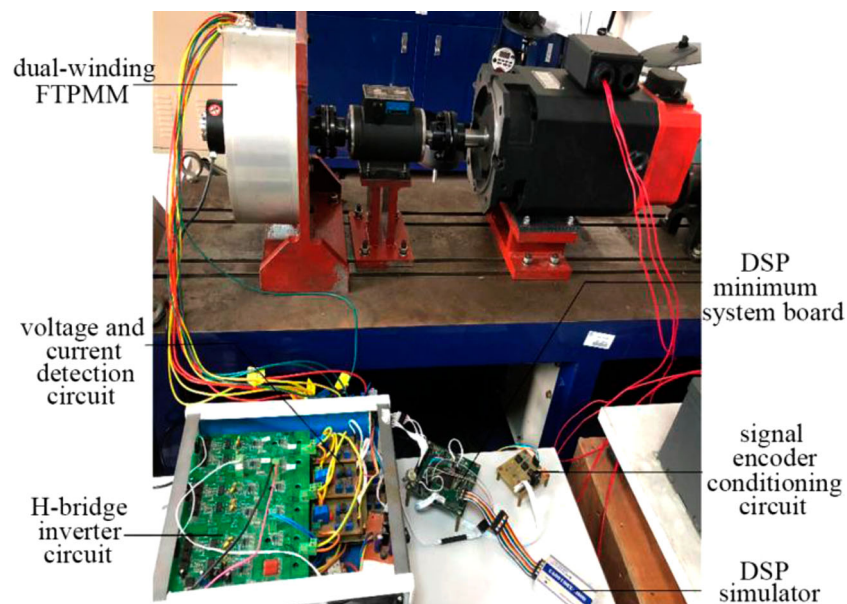
five-phase current starts to change with more harmonics when the motor opens one-phase at 0.25 s. After 0.25 s, the current vector tactics proposed in the literature [21] was adopted to redistribute the current to make the motor run stably. The estimated rotor position is close to the actual position with an error of  $\pm 0.02$  rad.

Figure 8 shows the simulation results of the rotor position estimation algorithm when the online identification function of motor parameters is adopted under the condition of two-phase open-circuit. When phase A and B opened at 0.25 s, the motor recovered to normal run by adopting fault-tolerant control strategy after 0.02 s. The position estimation error with two-phase open-circuit condition is slightly larger than single-phase open condition, but still within the range of  $\pm 0.02$  rad.

The simulation results show that the position error between the actual and the estimated is within the acceptable range when the FTPMM is working in



**Figure 8.** The simulation waveform of the speed step change under two-phase open-circuit fault condition. (a) The oscillograph of current of phase A, B, C: blue trace (A), red trace (B), yellow trace (C). (b) The oscillograph of current of phase A0, B0, C0: blue trace (A0), red trace (B0), yellow trace (C0). (c) The estimated rotor position and the actual position: blue trace (estimated position), purple trace (actual position). (d) The error of the estimated rotor position.



**Figure 9.** Experimental control system platform for the dual-winding FTPMM.

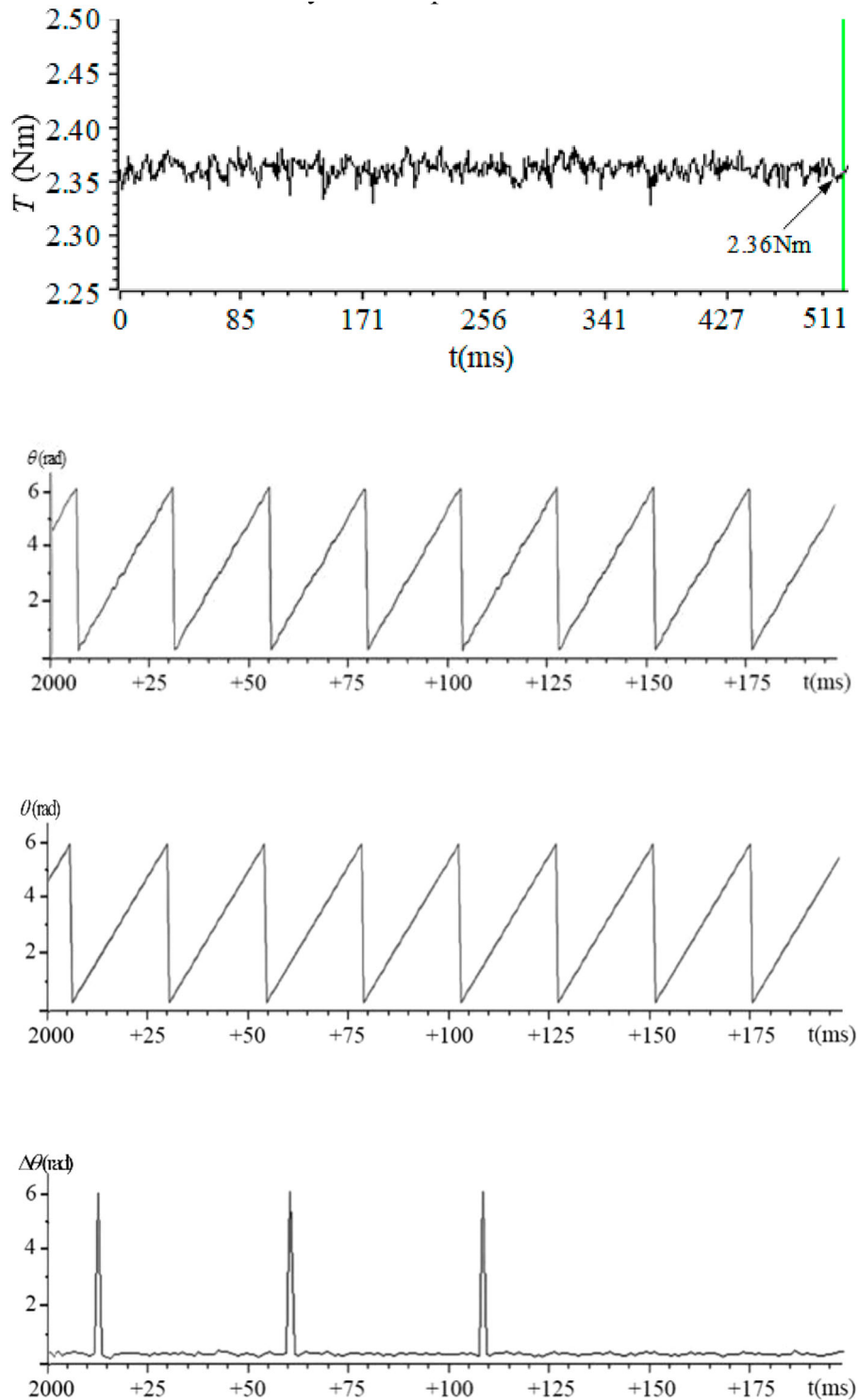


**Figure 10.** Experimental waveforms of healthy condition. (a) Output torque waveform. (b) Waveform of actual measured rotor position. (c) Waveform of estimated rotor position. (d) Waveform of rotor position error.

healthy, single-phase fault or even two-phase fault conditions, which proves the accuracy of the algorithm.

## 6. Experimental verification

In this paper, the accuracy and efficiency of the fault-tolerant control strategy and rotor position estimation algorithm are analyzed and testified in the laboratory using the hardware experiment platform of the dual-winding FTPMM.

Figure 9 shows the experimental platform; it mainly includes the dual-winding FTPMM, voltage and current detection circuit, digital signal processor (DSP) simulator, DSP minimum system board, signal encoder conditioning circuit and H-bridge inverter circuit.

EPWM1 is used in the control system to configure the reference time of the main programme and its frequency is set to 10 kHz. The current sampling period and the cycle time of CHBPWM controller both set to 100  $\mu$ s. Table 3 shows the main parameters of the motor.

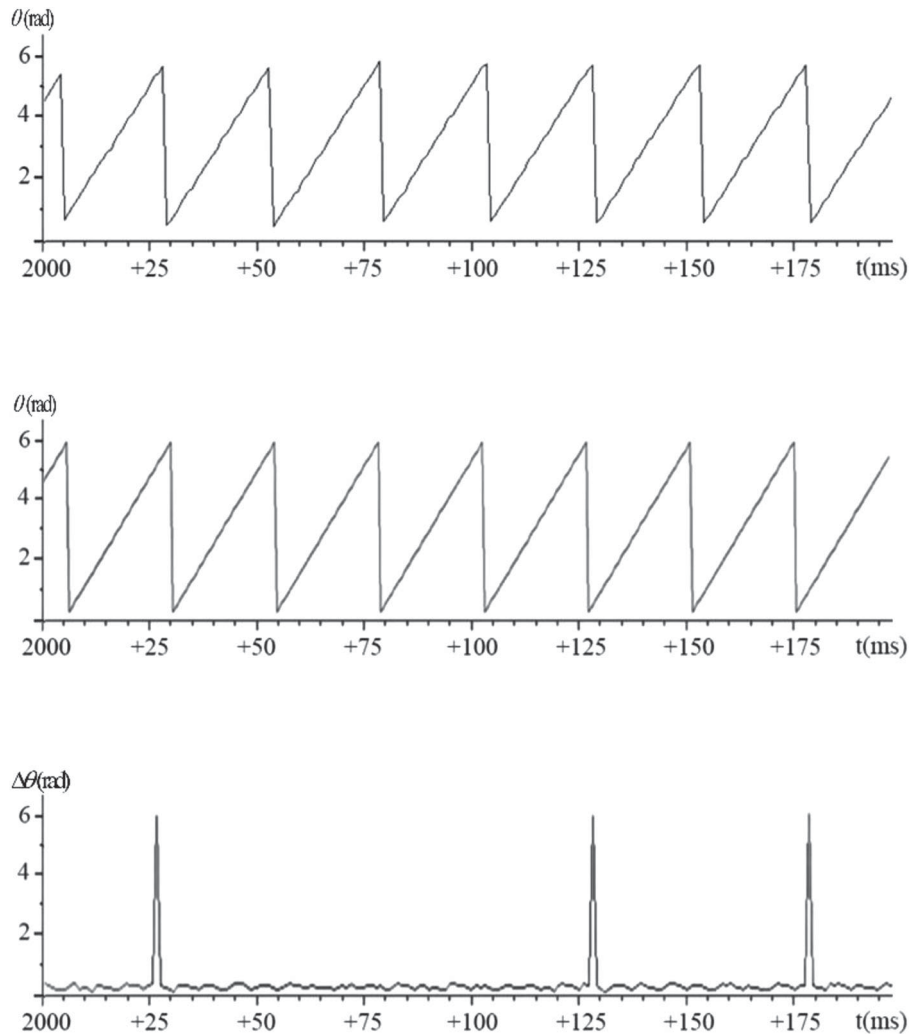


**Figure 11.** Experimental waveforms with phase A open-circuit fault occurs. (a) Waveform of the actual measured rotor position, (b) waveform of the estimated rotor position and (c) waveform of the rotor position error.

**Table 3.** Parameters of the dual-winding FTPMM.

Parameters	Values	Parameters	Values
Rated current (A)	3.14	Pole-pairs	4
Rated power (kW)	1.5	Number of slots	12
DC bus voltage (V)	100	Stator inductance (mH)	20
Rated speed ( $r \text{ min}^{-1}$ )	3000	Flux (Wb)	0.3
Stator resistance ( $\Omega$ )	1.59	Damping coefficient	0

The given speed and the load torque of the motor are set as 1000 r/min and 2.35 N m, respectively. It works under the condition of trouble-free experiment. The current waveform can be obtained by an oscilloscope, and other waveforms are outputted by CCS6.0 graph. Figure 10(a) is the output torque waveform. Figure 10(b) shows the actual rotor position measured by the encoder. Figure 10(c) is the estimated rotor position waveform based on the back-EMF estimation algorithm. Because of the limited sampling frequency, only part of the error waveform is captured. Figure 10(d) is the error waveform between estimated rotor position and actual rotor position. From the waveform, it can be seen that its value is between 0.2 rad to 0.4 rad, which is about 11–20°. The error is small but unsatisfactory for the position estimation result.

Use current vector fault-tolerant control tactics to obtain experimental results under the condition of analogue phase A open-circuit. The given speed of the motor is set to 1000 r/min. The waveform of the experimental results is shown in Figure 11. Figure 11(c) is the error waveform of estimated and actual rotor position. Similarly, only part of the error waveform is captured. The error is also about 15°, which has a relatively stable fault-tolerant effect.

The given speed of the motor is still set to 1000 r/min when the least-square parameter identification method with forgetting factor is introduced into the back-EMF position estimation algorithm. It can be seen from Figure 12(c) that the error between the estimated rotor position and actual rotor position is about 0° and not more than 5° fluctuation, which is a marked improvement over what it was before.

The given speed and the load torque of the motor which work under the condition of phase A open-circuit are set as 1000 r/min and 2.35 N m, respectively. Use the current vector fault-tolerant control tactics to obtain experimental results after introducing the parameter identification method into the back-EMF

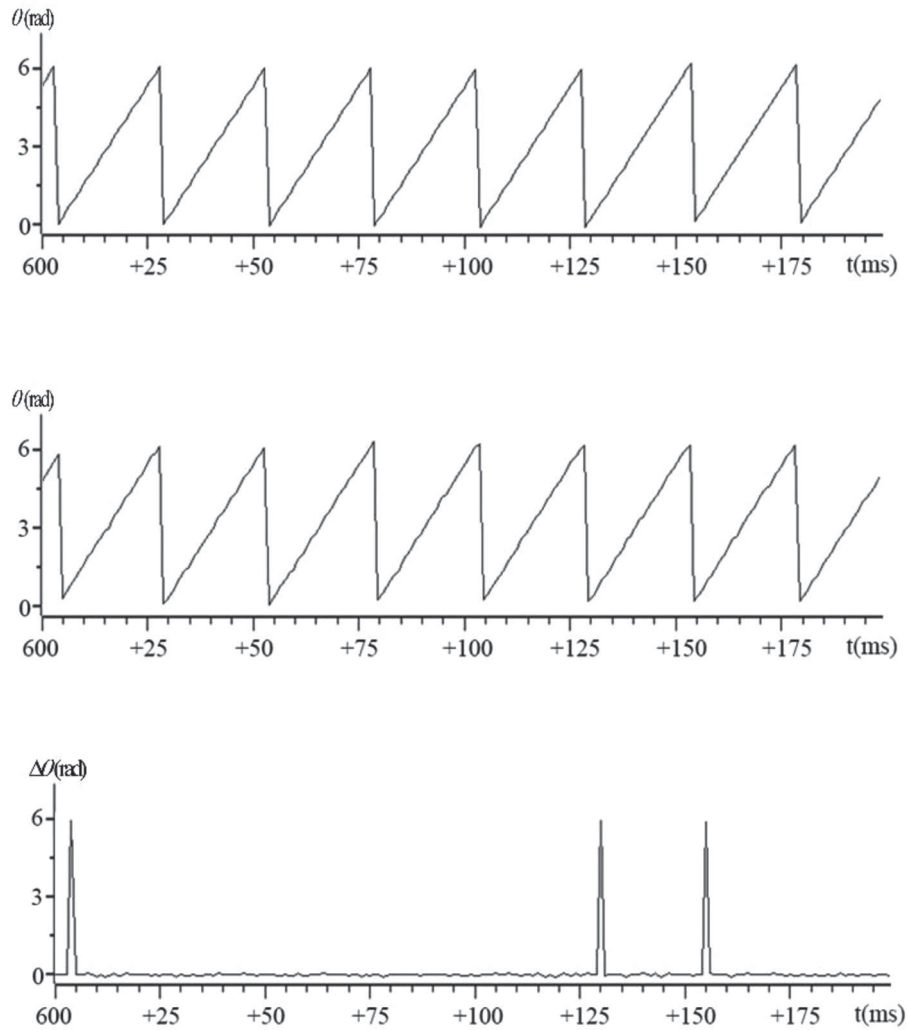


**Figure 12.** Experimental waveforms of healthy condition. (a) Waveform of the actual measured rotor position, (b) waveform of the estimated rotor position and (c) waveform of the rotor position error.

algorithm. The error between the estimated rotor position and the actual rotor position also fluctuates around  $0^\circ$  as shown in Figure 13(c). The result shows that the system fault-tolerant performance is good and the position estimation is more accurate.

The waveforms of the two groups experiment show that the estimated rotor position can be acquired using the back-EMF estimation algorithm under the healthy or fault condition and can be acquired accurately using the current vector fault-tolerant control tactic which base on back-EMF estimation algorithm under the condition of one-phase open-circuit. When the least-square parameter identification method with forgetting factor is introduced into the algorithm, whether there is a failure, more accurate rotor position can be obtained.

## 7. Conclusions

This paper analyzes the normal and fault tolerance operation of the dual-winding FTPMM. Based on the back-EMF method, a sensorless estimation method of rotor position for fault-tolerant motors is proposed.

The position of the rotor is estimated using the increment of magnetic linkage generated by each phase winding and the back-EMF of adjacent two phases, then the error compensation is carried out by the PLL technique. The forgetting factor recursive least-square method is introduced to improve the veracity of rotor position estimation. Using current vector fault-tolerant control strategy can improve the fault tolerance of the system. The position estimation method with the parameter identification function is simulated and verified under the condition of healthy and single-phase fault. It can be seen from the simulation results that the improved algorithm can measure the rotor position accurately whether the motor is working normally or fault conditions. Finally, hardware experiments show that the rotor position of dual-winding FTPMM can be obtained accurately through this algorithm, both under the condition of healthy and one-phase open-circuit. Besides, the FTPMM does not need to stop running and it can restore to normal operation quickly after taking effective fault-tolerant control strategy. The proposed position estimation algorithm and fault-tolerant control tactic for FTPMM can be

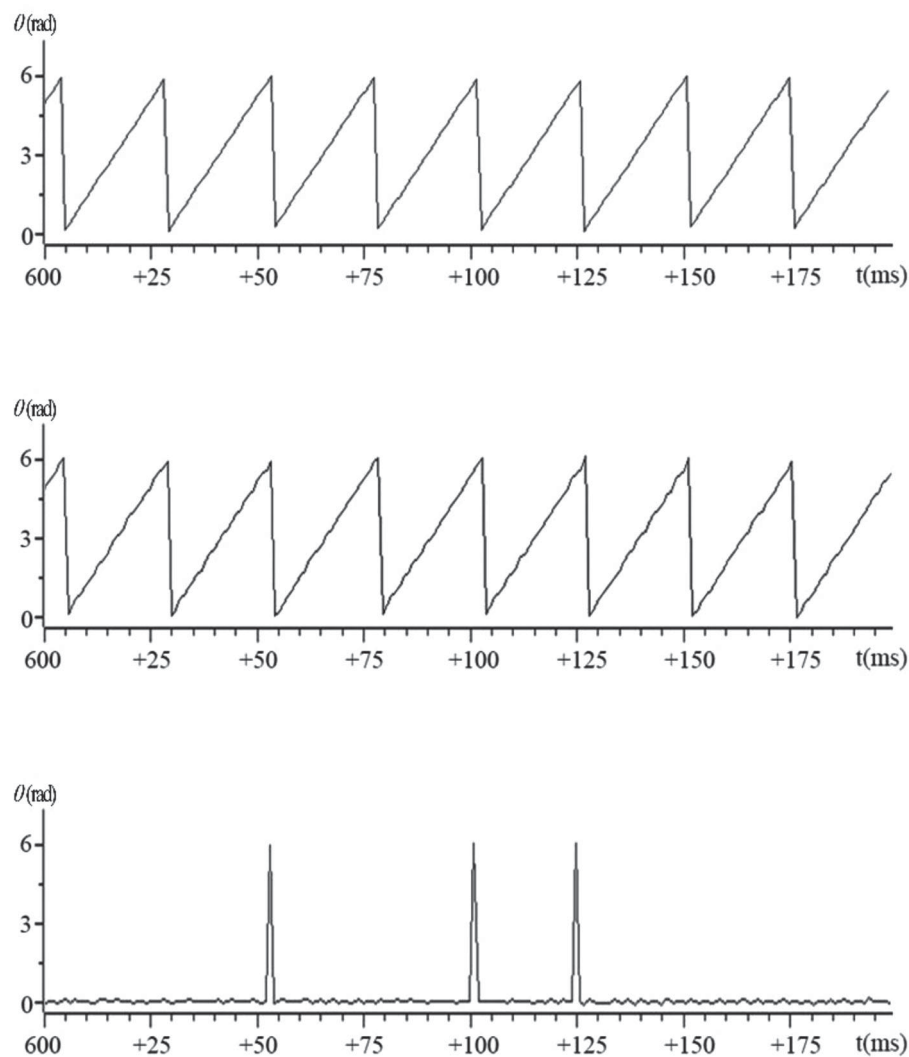


**Figure 13.** Experimental waveforms with phase A open-circuit fault occurs and the current vector fault-tolerant control strategy is applied. (a) Waveform of the actual measured rotor position, (b) waveform of the estimated rotor position and (c) waveform of the rotor position error.

expected to have a bright future in high reliability and high-power density applications, such as the fault-tolerant permanent magnet rim-driven motor which cannot be installed; the position sensor has been used in the shipbuilding industry.

### Disclosure statement

No potential conflict of interest was reported by the author(s).

### Funding

This work was supported by National Natural Science Foundation of China [Grant Number 51777024] and Dalian Science and Technology Innovation Fund [Grant Number 2018J12GX039].

### ORCID

Yonghan Liu  <http://orcid.org/0000-0002-0443-7395>

Jingwei Zhu  <http://orcid.org/0000-0002-1737-3108>

Zhibin Wang  <http://orcid.org/0000-0002-8588-7143>

Yan Liang  <http://orcid.org/0000-0003-4798-1152>

### References

- [1] Jiang X, Huang W, Cao R, et al. Analysis of a dual-winding fault-tolerant permanent magnet machine drive for aerospace applications. *IEEE Trans Magn.* 2015;51(11):1–4.
- [2] Zhang F, Zhu J, Liu D. Modeling and simulation of six-phase fault-tolerant permanent magnet motor vector control system. Harbin, China. *Power electronics and motion control conference*; IEEE; 2012. p. 1319–1323.
- [3] Kumar R, Das S, Syam P, et al. Review on model reference adaptive system for sensorless vector control of induction motor drives. *IET Electr Power Appl.* 2015;9(7):496–511.
- [4] Ma S, Wu P, Ji J, et al. Sensorless control of salient PMSM with adaptive integrator and resistance online identification using strong tracking filter. *Int J Electron.* 2016;103(2):217–231.
- [5] Liang J, Zhang X, Qiao M, et al. Optimal design and multifield coupling analysis of propelling motor used in a novel integrated motor propeller. *IEEE Trans Magn.* 2013;49(12):5742–5748.
- [6] Wang Y, Li K, Liu X. Improved deadbeat control for PMSM with terminal sliding mode observer. 2019 22nd international conference on electrical machines

- and systems (ICEMS); Harbin, China; 2019. p. 1–5.
- [7] Zhao H, Luo P, Wang N, et al. Fuzzy logic control of the fault-tolerant PMSM servo system based on MRAS observer. 2018 Chinese control and decision conference (CCDC); Shenyang; 2018. p. 1812–1817.
- [8] Bourogaoui M, Sethom HBA, Belkhdja IS. Real-time encoder faults detection and rotor position estimation for permanent magnet synchronous motor drives fault tolerant sensorless control using digital signal controller. *Math Comput Simul.* 2015;131(18):253–267.
- [9] Diaz Reigosa D, Fernandez D, Zhu Z, et al. PMSM magnetization state estimation based on stator-reflected PM resistance using high-frequency signal injection. *IEEE Trans Ind Appl.* 2015;51(5):3800–3810.
- [10] Luo X, Tang Q, Shen A, et al. PMSM sensorless control by injecting HF pulsating carrier signal into estimated fixed-frequency rotating reference frame. *IEEE Trans Ind Electron.* 2016;63(4):2294–2303.
- [11] Celik H, Yigit T. Field-oriented control of the PMSM with 2-DOF PI controller tuned by using PSO. 2018 international conference on artificial intelligence and data processing (IDAP); Malatya, Turkey; 2018. p. 1–4.
- [12] Pajchrowski T. Application of neural networks for compensation of torque ripple in high performance PMSM motor. 2017 19th European conference on power electronics and applications (EPE'17 ECCE Europe); Warsaw; 2017. p. 1–8.
- [13] Zhan H, Zhu ZQ, Odavic M. Nonparametric sensorless drive method for open-winding PMSM based on zero-sequence back EMF with circulating current suppression. *IEEE Trans Power Electron.* 2017;32(5):3808–3817.
- [14] de Paula GT, de A. Monteiro JRB, de Alvarenga BP, et al. On-load back EMF of PMSM using Maxwell stress tensor. *IEEE Trans Magn.* 2016;54(7):1–15.
- [15] Liu JM, Zhu ZQ. Improved sensorless control of permanent-magnet synchronous machine based on third-harmonic back EMF. *IEEE Trans Ind Appl.* 2014;50(3):1861–1870.
- [16] Sun X, Hu C, Lei G, et al. Speed sensorless control of SPMSM drives for EVs with a binary search algorithm-based phase-locked loop. *IEEE Trans Veh Technol.* 2020;69(5):4968–4978.
- [17] Sun X, Cao J, Lei G, et al. Speed sensorless control for permanent magnet synchronous motors based on finite position set. *IEEE Trans Ind Electron.* 2020;67(7):6089–6100.
- [18] Xu J, Du Y, Fang H, et al. A robust observer and nonorthogonal PLL-based sensorless control for fault-tolerant permanent magnet motor with guaranteed postfault performance. *IEEE Trans Ind Electron.* 2020;67(7):5959–5970.
- [19] Ying L, Ertugrul N. A novel, robust DSP-based indirect rotor position estimation for permanent magnet AC motors without rotor saliency. *IEEE Trans Power Electron.* 2003;18(2):539–546.
- [20] Sun P, Ge Q, Zhang B, et al. Sensorless control technique of PMSM based on RLS on-line parameter identification. 2018 21st international conference on electrical machines and systems (ICEMS); Jeju; 2018. p. 1670–1673.
- [21] Mohammadpour A, Parsa L. Global fault-tolerant control technique for multiphase permanent-magnet machines. *IEEE Trans Ind.* 2015;51:178–186.
- [22] An JS, Ertugrul N, Soong WL, et al. An indirect rotor position estimation technique for a fault-tolerant brushless PM motor drive. 2008 IEEE power electronics specialists conference; Rhodes; 2008. p. 1553–1558.
- [23] Xu J, Du Y, Fang H, et al. A robust observer and nonorthogonal PLL-based sensorless control for fault-tolerant permanent magnet motor with guaranteed postfault performance. *IEEE Trans Ind Electron.* 2020;67(7):5959–5970.
- [24] Wu, Zhao CY, Sun M. Enhancing low-speed sensorless control of PMSM using phase voltage measurements and online multiple parameter identification. *IEEE Trans Power Electron.* 2020;35(10):10700–10710.
- [25] Feng D-Z, Bao Z, Jiao L-C. Total least mean squares algorithm. *IEEE Trans Signal Process.* 1998;46(8):2122–2130.
- [26] Song Q, Mi Y, Lai W. A novel variable forgetting factor recursive least square algorithm to improve the anti-interference ability of battery model parameters identification. *IEEE Access.* 2019;7:61548–61557.
- [27] Zhu J, Bai H, Wang X, et al. Current vector control strategy in a dual-winding fault-tolerant permanent magnet motor drive. *IEEE Trans Energy Convers.* 2018;33(4):2191–2199.